ULTRASONIC IMAGING 23, 73-89 (2001)

Filter-Based Synthetic Transmit and Receive Focusing

MENG-LIN LI AND PAI-CHI LI

Department of Electrical Engineering
National Taiwan University
Tapei, Taiwan, R.O.C.
email: paichi@cc.ee.ntu.edu.tw

Most diagnostic ultrasonic imaging systems perform fixed focusing on transmit and dynamic focusing on receive. Such systems suffer from image quality degradation at depths away from the transmit focal zone. Several dynamic transmit focusing techniques have been previously investigated. Among them, a filter-based, retrospective focusing technique was proposed to increase the length of the transmit focal zone. In this paper, the filter-based technique is extended from dynamic receive focusing to fixed receive focusing. It is shown that the filtering technique with fixed receive focusing can achieve an image quality similar to that of dynamic receive focusing with filtering. The performance of the proposed approach is verified using real ultrasound data. It is shown that the proposed approach with fixed receive focusing requires a longer filter than that with dynamic receive focusing. Nonetheless, system complexity is greatly reduced with synthetic transmit and receive focusing because the dynamic receive focusing circuit is no longer needed.

KEY WORDS: Deconvolution; depth of focus; dynamic focusing; optimal filter; synthetic aperture.

I. INTRODUCTION

Most current real-time array imaging systems perform fixed focusing on transmit and dynamic focusing on receive. The focusing quality of such systems is less than optimal at imaging depths away from the transmit focal zone. To fully realize the image quality potentially achievable by an array imaging system, dynamic transmit focusing is desired. Various methods have been proposed to increase the length of the transmit focal zone. One straightforward method is to simply apodize the transmit aperture. However, apodization extends the transmit focal zone at the price of lateral resolution.[1] Another method based on nondiffracting beam propagation was proposed by Lu and Greenleaf.[2-4] Although nondiffracting beams produce a longer transmit focal zone, high sidelobes are introduced and, thus, the contrast resolution is affected.

Coded excitation methods have also been proposed for dynamic transmit focusing.[5,6] In this case, independent codes are used to excite individual channels of a phased array. An image can then be reconstructed by using a pseudo-inverse linear operator based on singular value decomposition. Note that the image quality is determined by the orthogonality among the transmit codes. Unfortunately, orthogonality is usually poor due to the limited time-bandwidth product of current medical ultrasound transducers. Synthetic transmit focusing using weighting has also been proposed.[7,8] Transmit foci are synthesized between two physical focal points by summing the weighted echoes returning from transmissions corresponding to the two real focal points. The weights are determined based on a least-squares method that minimizes the combined phase errors. However, multiple firings are needed to improve the focusing quality between two original focal points. Thus, the frame rate is reduced. In addition, only the image quality between the two physical focal points can be improved.

Bae and Jeong proposed a delay-and-sum based synthetic aperture imaging method with virtual source elements.[9] The method synthesizes dynamic two-way (i.e., transmit and re-

0161-7346/01 $18.00

ceive) focusing with a linear array transducer. It improves the lateral resolution and sidelobe levels at all imaging depths. Nonetheless, it is susceptible to motion artifacts. Finally, a retrospective dynamic transmit focusing technique suitable for real-time applications was proposed by Freeman et al.[10] The retrospective filtering technique treats dynamic focusing as a deconvolution problem and the length of the transmit focal zone is extended by filtering the predetection image data. Note that the previous work was based on fixed transmit and dynamic receive focusing. Fixed transmit and fixed receive focusing was not considered. As will be shown in this paper, fixed receive focusing with filtering can provide similar imaging performance to that of dynamic receive focusing. Since only fixed receive focusing is employed, the system complexity is substantially reduced.

In this paper, the retrospective filtering technique is reviewed in section II. The characteristics of the pulse-echo effective aperture with fixed receive focusing are then compared to those with dynamic receive focusing in section III. In section IV, the performance of retrospective transmit and receive focusing is compared to that of retrospective transmit focusing using real ultrasound data. The paper concludes in section V.

II. REVIEW OF RETROSPECTIVE FILTERING TECHNIQUE

An image can be viewed as the convolution of a pulse-echo point spread function with a scattering distribution function. In the lateral direction, the pulse-echo point spread function is the multiplication of the transmit beam and the receive beam. The retrospective filtering technique treats dynamic focusing as a deconvolution problem. In other words, synthetic focusing is done by laterally applying a filter to the beam data.[10] Such a filter is range dependent and needs to be applied after beam formation and before envelope detection. Furthermore, the filter has complex coefficients if the beam sum signal is demodulated to baseband. In other words, we have

$$\underbrace{(S \otimes B_{oof})}_{\text{original image}} \otimes \underbrace{(B_{ideal} \otimes^{-1} B_{oof})}_{\text{inverse filter}} = \underbrace{S \otimes B_{ideal}}_{\text{focused image}} \quad (1)$$

where $\otimes$ represents convolution, $\otimes^{-1}$ denotes deconvolution, S is the scattering distribution function, B_{oof} is the out-of-focused pulse-echo beam pattern and B_{ideal} is the ideal pulse-echo beam pattern (i.e., dynamic focusing on both transmit and receive). For a sector image, all the above terms are a function of $(R, \sin\theta)$, where R is the range and θ is the steering angle.

The inverse filter in Eq. (1) deconvoles the out-of-focused beam into a focused beam. Based on the discrete space Fourier transform relationship between a beam pattern and the corresponding aperture function, it is straightforwd to see that spectrum of the inverse filter is the ideal pulse-echo effective aperture divided by the out-of-focused pulse-echo aperture function. The aperture function can also be used to represent the spatial frequency spectrum. Thus, the purpose of the inverse filter is to change the amplitude and the phase of an out-of-focused aperture function into an ideal aperture function.

Robust results can be obtained using the inverse filter only if there are no singular points (i.e., points with small amplitudes) and the SNR is sufficiently high. Otherwise, direct application of the inverse filter amplifies the noise and degrades the beam quality. In addition, the inverse filter with the number of taps equaling the number of beams in the image is also not practical. Hence, an alternative filtering approach based on a minimum mean squared error criterion is used.[10-13] The filter is also known as the optimal filter in the sense that the mean

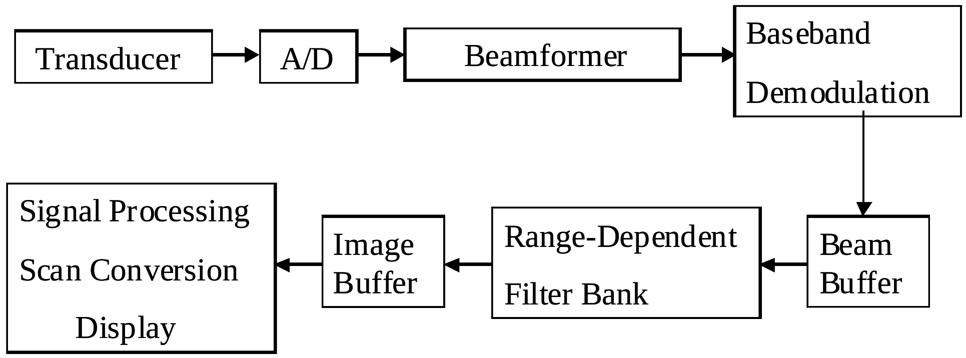

FIG. 1 Hardware structure for retrospective focusing.

squared error between the filter output and a desired beam pattern is minimized. The desired beam pattern is typically the dynamically-focused beam at the same image position.

Let the column vector $\underline{d}$ represent the desired beam pattern, the column vector $\underline{b}$ be the out-of-focused beam pattern and the column vector $\underline{f}$ describes the filter coefficients. Then the mean squared error can be defined as

$$\varepsilon = (B\underline{f} - \underline{d})^H (B\underline{f} - \underline{d}) \tag{2}$$

where H denotes the Hermitian conjugate and $B\underline{f}$ is the matrix representation of the convolution of $\underline{b}$ and $\underline{f}$. Therefore, the optimal filter that minimizes the mean squared error can be found as

$$\underline{f}^{opt} = (B^H B)^{-1} B^H \underline{d} \tag{3}$$

As mentioned by Freeman et al, longer filters are required for ranges farther away from the focus.[10] The efficacy of the retrospective filtering technique using the optimal filter has also been demonstrated and a 2-7dB sidelobe reduction was achieved with unapodized apertures.

A system block diagram for retrospective focusing is illustrated in figure 1.[10-12] After the echo signal is received and digitized by the A/D converter, the beamformer properly delays the data before the beam sum is demodulated to baseband and stored in the beam buffer. The range-dependent filter then retrospectively synthesizes a focused beam and the data is sent to the image buffer for further signal processing, scan conversion and display. Note that a pipeline structure can be used for implementation of these range-dependent complex filters. The complex filters have lengths varying as a function of range and coefficients are precalculated and stored in the filter bank. This architecture is similar to the wall filter architecture in color Doppler imaging modes.

III. PULSE-ECHO EFFECTIVE APERTURES

As previously mentioned, the optimal filter or the inverse filter converts a distorted pulse-echo aperture function into an ideal one. Effectiveness of the filter is primarily determined by characteristics of the aperture function and the filter length. First, the effective

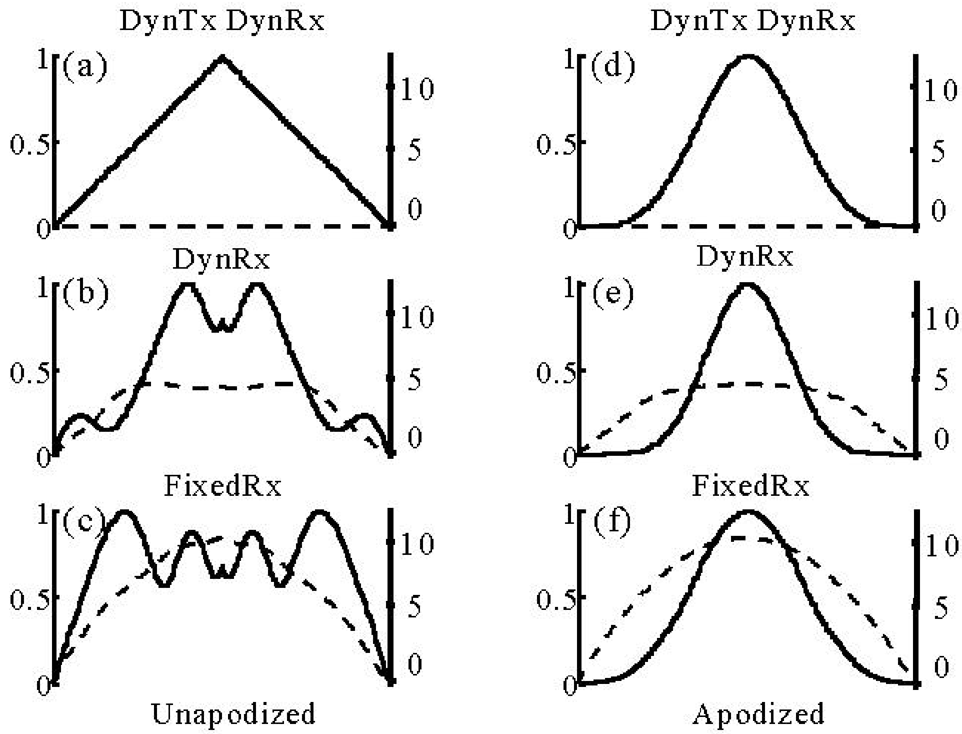

FIG. 2 Pulse-echo effective aperture functions (solid is the magnitude, dashed is the phase). For each panel, the left vertical axis is for the amplitude and the right vertical axis is for the phase (in radians). Panels on the left show cases without apodization and panels on the right are cases with apodization. (a) and (d) are ideal pulse-echo apertures. (b) and (e) are pulse-echo apertures with fixed transmit and dynamic receive focusing. (c) and (f) are pulse-echo apertures with fixed transmit and fixed receive focusing.

width of the aperture function fundamentally limits the width of the filtered beam. The wider that the aperture is, the narrower the beam width that can be achieved. Second, singular points within the aperture affect robustness of the deconvolution process. To evaluate the performance of the filter-based approach, pulse-echo effective apertures with fixed transmit and fixed receive focusing are studied and compared to those with fixed transmit and dynamic receive focusing.

Without loss of generality, a 1-D array focused at range R_0 and zero steering angle is assumed. Further, assuming continuous wave propagation, the phase ϕ_n of the one-way aperture at range R can be written as[1]

$$\phi_n = k\,\frac{x_n^2}{2}\left(\frac{1}{R} - \frac{1}{R_0}\right) \tag{4}$$

where k is the wave number and x_n is the distance between the n-th element and the array center. Note that the phase is equal to zero at the focal depth, whereas quadratic phase across the aperture exists in the out-of-focused region. In other words, fixed focusing results in different quadratic phases at different ranges. Since the convolution of transmit and receive apertures is the pulse-echo effective aperture, the quadratic phase distorts the pulse-echo effective aperture and possibly generates singular points. In the examples shown below, a

128 element 1-D array with a 3.5 MHz center frequency and half-wavelength pitch is assumed. The sound velocity is 1.48 mm/µs.

Effects of the quadratic phase on the pulse-echo aperture function are illustrated in figure 2. Effective apertures at range 80 mm are shown. The left panels show examples of unapodized apertures. The top panel (a) shows the pulse-echo ideal aperture (i.e., with both transmit and receive focused at 80 mm). Since an unapodized one-way aperture (i.e., transmit or receive only) at the focal point is rectangular with zero phase, the pulse-echo ideal aperture is triangular (solid) also with zero phase (dashed). The vertical axis shown on the left of each panel is the normalized amplitude and the vertical axis shown on the right is the phase (in radians). The middle panel (b) shows the pulse-echo effective aperture with fixed transmit focusing at 60 mm and dynamic receive focusing (i.e., the receive beam is focused at 80 mm). The bottom panel (c) shows the effective pulse-echo aperture with fixed transmit and fixed receive focusing, both at 60 mm. Apparently, both pulse-echo effective apertures in (b) and (c) are distorted (i.e., with amplitude variations and non-zero phase) due to the quadratic phase in the one-way aperture function. Since both apertures in panels (b) and (c) have no zeros in the middle portion of the aperture function, one can define the passband of the spatial frequency spectrum (i.e., the pulse-echo aperture function) as the region where the amplitude is higher than a certain threshold (e.g., -6 dB from the maximum). The width of the passband can be used to evaluate the effectiveness of the filtering technique. In figure 2, because the –6 dB aperture width in panel (c) is larger than that of the ideal aperture in panel (a), the filter is generally a spatial lowpass filter (LPF) and is less susceptible to noise compared to a highpass filter (HPF).

The right panels of figure 2 show the pulse-echo effective apertures with Hamming apodization. In this case, the apodized apertures have less amplitude variations compared to the unapodized apertures. This indicates that the filter design with fixed receive focusing is easier with apodization. For dynamic receive focusing, the effective aperture in panel (e) is narrower than the ideal one in panel (d). Hence, noise will be amplified when the filter is applied. Also, the filtering technique with fixed receive focusing is expected to outperform that with dynamic receive focusing since the –6 dB width in panel (f) is larger than that in panel (e).

The -6 dB and –30 dB aperture widths of pulse-echo effective apertures for a target at range 80 mm are shown in figure 3. The widths are normalized to the corresponding widths of the ideal aperture function. The –6 dB width is used to represent the effective aperture width and the expected beam width after a filter is properly applied. The –30 dB width, on the other hand, is also adopted since the inverse filter becomes unreliable when low level signals are amplified. The horizontal axis is the fixed transmit focal depth. For dynamic receive focusing, the receive focal depth is the same as the target depth (i.e., 80 mm). For fixed transmit and fixed receive focusing, the horizontal axis represents both the transmit and the receive focal depths. The solid line in each panel corresponds to fixed transmit and dynamic receive focusing and the dashed line corresponds to fixed transmit and fixed receive focusing. The left panels (i.e., (a) and (b)) show cases without apodization and the right panels (i.e., (c) and (d)) are cases with apodization.

Figure 3(a) shows the normalized –6 dB width of the pulse-echo effective aperture. With fixed transmit and fixed receive focusing, the width is always larger than the width of the ideal aperture. For dynamic receive focusing, on the other hand, the normalized –6 dB aperture widths become smaller than one when it is away from the target depth. Results for the apodization cases shown in figure 3(c) are similar with the exception that the –6 dB width for fixed transmit and fixed receive focusing are relatively constant compared to those without apodization. Figure 3(b) shows the –30 dB width without apodization. The difference between fixed receive focusing (dashed) and dynamic receive focusing (solid) is smaller than

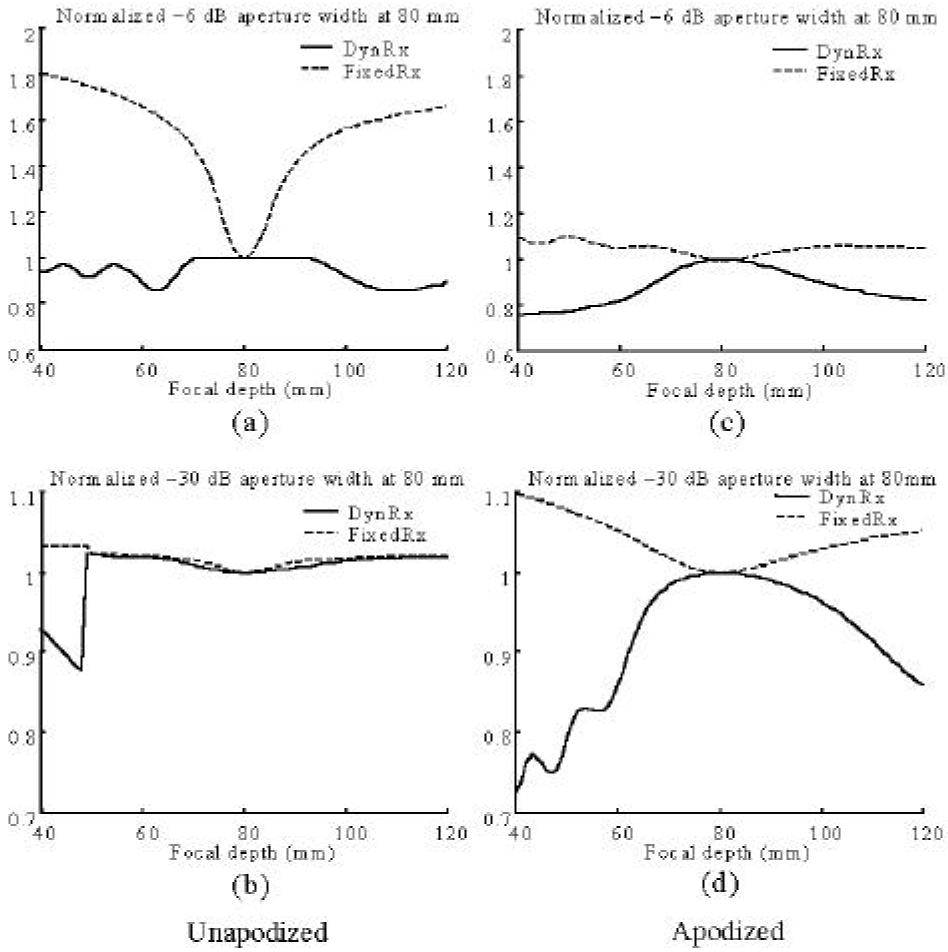

FIG. 3 (a) and (c) are normalized –6 dB aperture widths. (b) and (d) are normalized –30 dB widths. Solid line corresponds to fixed transmit and dynamic receive focusing. Dashed line corresponds to fixed transmit and fixed receive focusing. (a) and (b) are without apodization. (c) and (d) are with apodization.

that shown in figure 3(a). The difference in the –30 dB width becomes more noticeable when apodization is applied, as shown in figure 3(d). Note that with apodization, the –6 dB width and the –30 dB width are similar.

Apertures with fixed transmit and fixed receive focusing at 60 mm at different target ranges (69 mm, 81 mm, 98 mm) are shown in figure 4. The left panels show the unapodized cases and the right panels show the apodized cases. Figures 4(a) and 4(b) show that as the target moves further away from the focal zone, the pulse-echo effective aperture becomes wider. Moreover, both amplitude variations and the quadratic phase error also increase. Note that the relationship between magnitude of the quadratic phase and the aperture width is similar to the relationship between the phase of a chirp signal and the corresponding spectral bandwidth.[13] In figures 4(c) and 4(d), the apodized effective apertures are noticeably different from the unapodized cases in that the amplitude variations at different ranges are not as significant. In both cases, a longer filter is required to remove the defocusing effect for a range farther away from the focal depth due to the larger phase error and/or the larger amplitude variations.

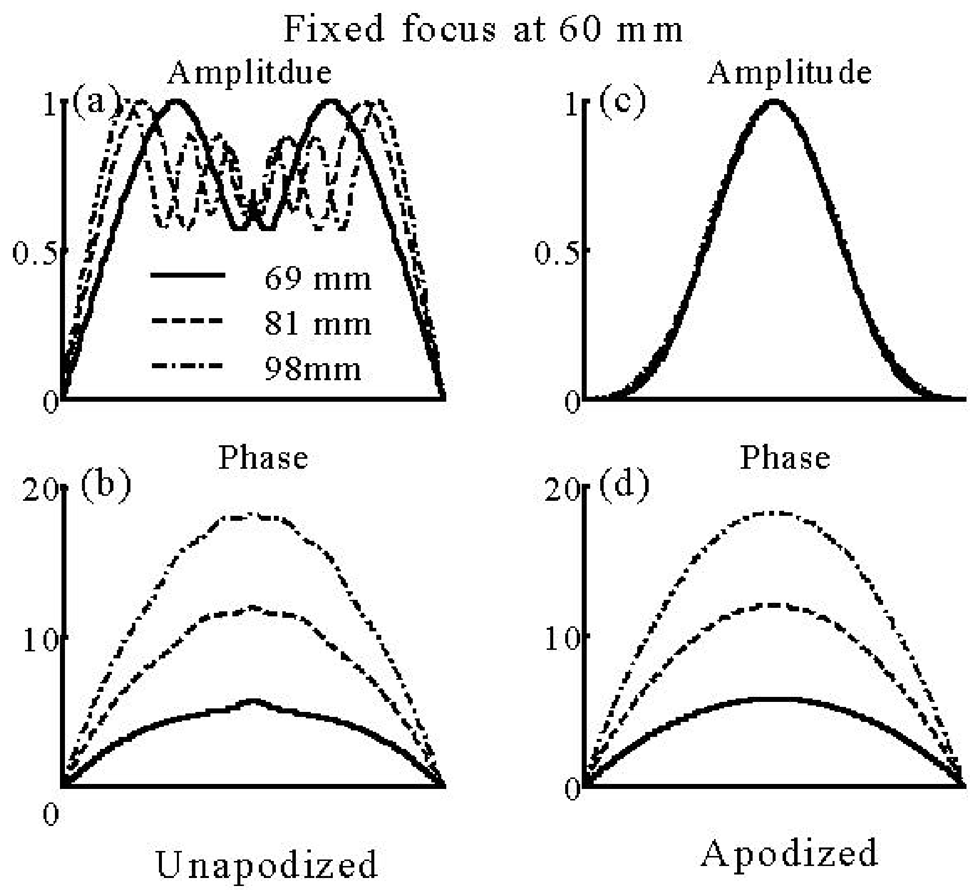

FIG. 4 Apertures at target ranges 69 mm, 81 mm and 98 mm with fixed transmit and fixed receive focal depth at 60 mm. Left panels are without apodization and right panels are with apodization. (a) and (c) are for amplitudes. (b) and (d) are for phases.

Results shown in figure 3 were generalized in figure 5 by considering all possible combinations of the transmit and the receive focal depths. Panels (a) and (b) are the unapodized cases and panels (c) and (d) show the apodized cases. The horizontal axis is the transmit focal depth, the vertical axis represents the receive focal depth and the target depth is fixed at 80 mm. The image brightness is the normalized –6 dB aperture width in figures 5(a) and 5(c), whereas the image brightness is the normalized –30 dB width in figures 5(b) and 5(d). The following observations are made. First, both the –6 dB and the –30 dB widths are largest along the diagonal (upper left to lower right) where the transmit and receive focal depths are the same. Second, the horizontal line with the receive focus at 80 mm represents fixed transmit and dynamic receive focusing since the target depth is also at 80 mm. Third, the upper right region corresponds to the cases where the transmit focus is deeper and the receive focus is shallower than the target depth. Fourth, the lower left region represents the cases that the transmit focus is shallower and the receive focus is deeper than the target depth. In all cases, fixed transmit and fixed receive focusing at the same depth has the largest width. Thus, the best performance is expected.

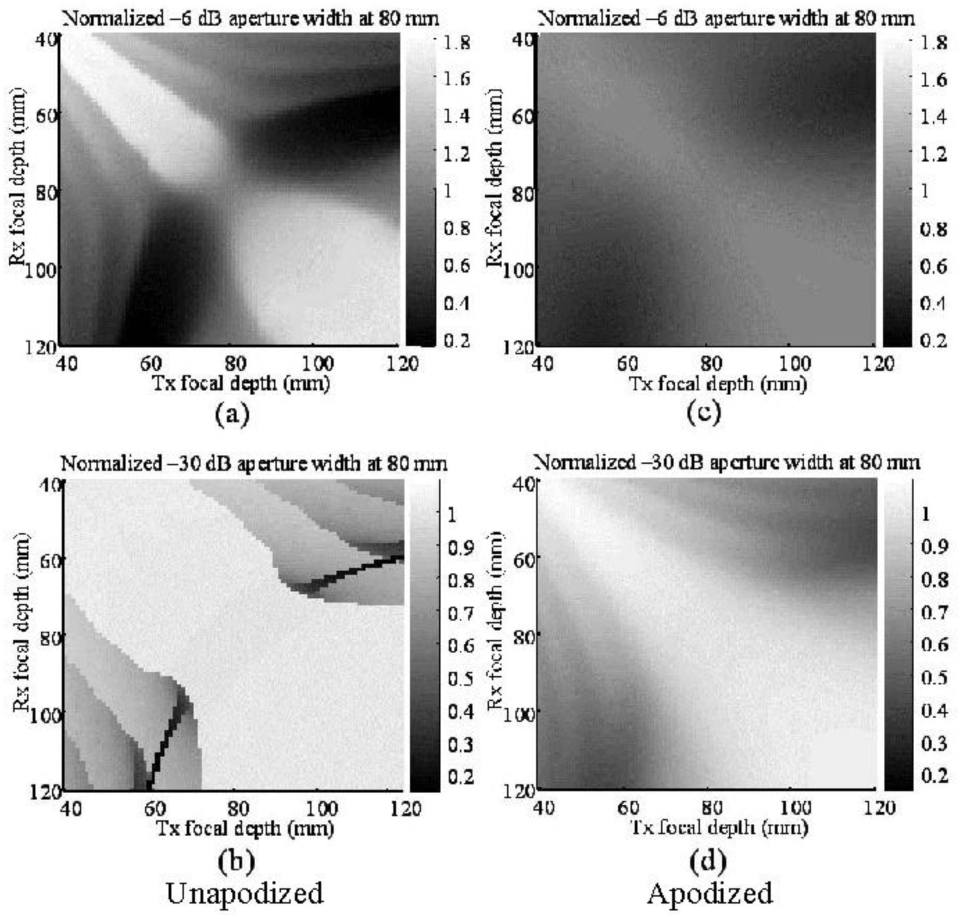

FIG. 5 (a) and (c) are the normalized –6 dB aperture widths. (b) and (d) are normalized –30 dB aperture widths. The vertical axis is the receive focal depth and the horizontal axis is the transmit focal depth. (a) and (b) are without apodization. (c) and (d) are with apodization.

IV. EXPERIMENTAL RESULTS

Simulated images using real ultrasound data are presented in this section. All the raw data are available at the web site *bul.eecs.umich.edu.* They were acquired using a 128-element, 3.5MHz phased array transducer (Acuson V328, Mountain View, California, U.S.A.). Data from a wire and tissue-mimicking phantom were used. The wire phantom consisted of six nylon wires in water and an independent optimal filter was derived for each wire. Each filter was then applied to a zone extending over a range of 20 mm with the wire at the center. The six wires were at ranges of 34, 48, 65, 83, 101 and 121 mm, respectively. For all images, a transmit f/number of 2 and a receive f/number of 1.5 were applied. For all apodized cases, the Hamming window was used on both transmit and receive. Cases corresponding to fixed focal depths at 60 mm and 120 mm were investigated.

Figure 6 shows the mean-squared error, defined in Eq. (2) as a function of the filter length, for the four wires at 65 (lines with circles), 83 (lines with crosses), 101 (lines with squares) and 121mm (lines with triangles). Nyquist beam spacing was used. Panel (a) is for dynamic

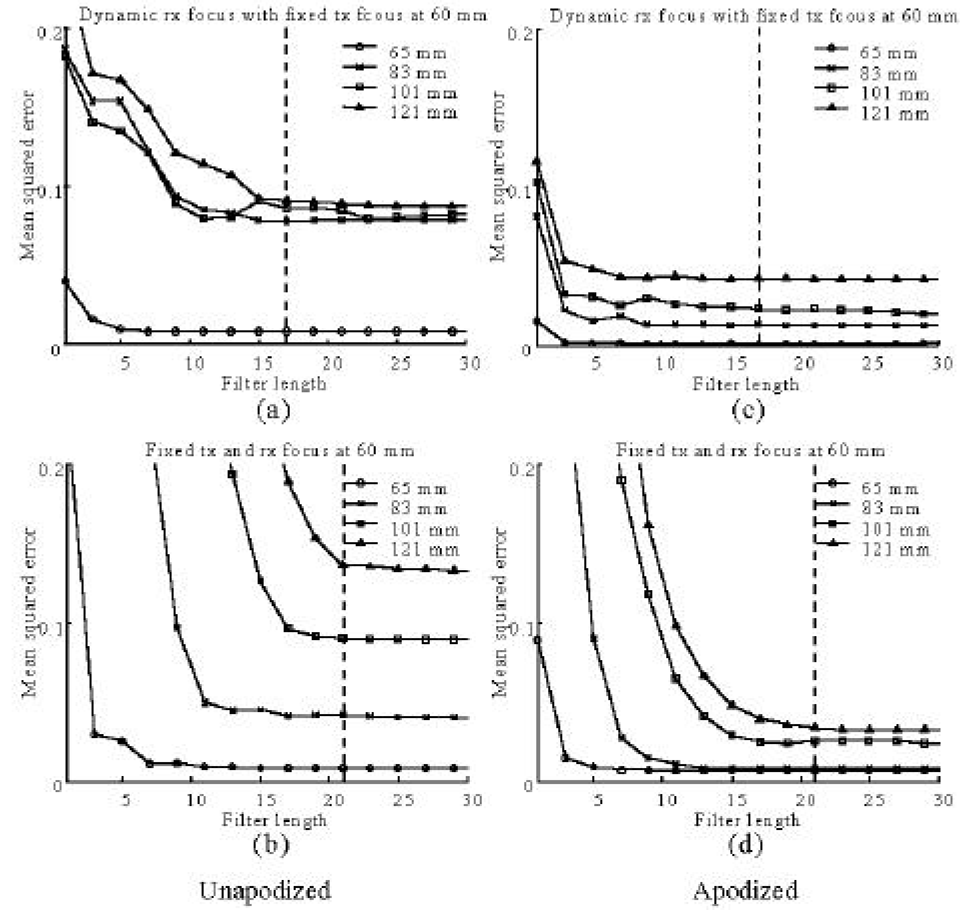

FIG. 6 Mean-squared error as a function of the filter length. Left panels show the unapodized cases and right panels show the apodized cases. (a) and (c) are dynamic receive focusing with fixed transmit focusing at 60 mm. (b) and (d) fixed transmit and fixed receive focusing at 60 mm.

receive focusing with fixed transmit focusing at 60 mm. Panel (b) is for fixed transmit and fixed receive focusing at 60 mm. Both panels correspond to results without apodization. As indicated in the figures, the error generally decreases and reaches a minimum as the filter length increases. Moreover, a longer filter is required for the wire farther away from the focal depth to reach the minimum. Such results are consistent with the spatial frequency spectra shown in figure 4 and the discussion in the previous section. The minimum mean squared errors acquired in (b) are generally higher than those in (a), except for the wire at 83 mm.

Figures 6(c) and 6(d) show the apodized cases. Different from the unapodized cases, the filter length required to reach the minimum mean squared error is smaller for both dynamic and fixed receive focusing. This is because the amplitude variations of the apodized apertures are smaller than those of the unapodized apertures, as shown in figure 2. Therefore the filter design becomes easier with apodization. In addition, the minimum mean-squared errors for fixed focusing (in (d)) are generally slightly lower than those with dynamic receive focusing (in (c)), except for the wire at 65 mm. This is again consistent with the results shown in figure 2 in that with apodization, the width of the aperture for dynamic receive fo-

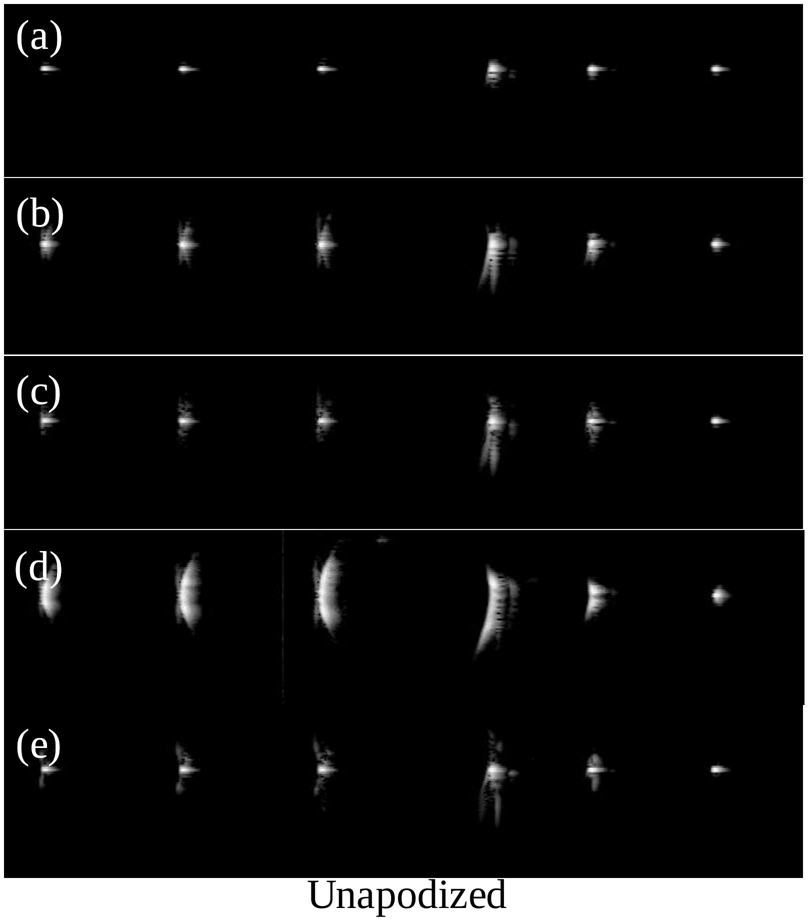

FIG. 7 Images of six wires over a 40 dB dynamic range (unapodized). The vertical axis is the azimuth and the horizontal axis represents the range. (a) is dynamic transmit and dynamic receive focusing. (b) is fixed transmit focusing at 60 mm and dynamic receive focusing. (c) is (b) with the retrospective filtering technique. (d) is fixed transmit and fixed receive focusing at 60 mm. (e) is (d) with the retrospective filtering technique.

cusing is smaller than that for fixed receive focusing. Therefore, filtering with fixed receive focusing is more efficient but a longer filter is needed. Based on figure 6, a filter length of 17 was applied for dynamic receive focusing and a filter length of 21 was used for fixed receive focusing in the following results. Nonetheless, a smaller filter length could have been used in the apodized cases.

Figure 7 shows 40 dB images of the wire phantom for dynamic transmit and dynamic receive focusing (panel (a)), fixed transmit focusing at 60 mm and dynamic receive focusing before filtering (panel (b)) and after filtering (panel (c)), fixed transmit and fixed receive focusing at 60 mm before filtering (panel (d)) and after filtering (panel (e)). All images are without apodization. Note that the images are sector scan images prior to scan conversion and the different wires along different directions are aligned along the same line for ease of display. The vertical axis is the azimuth and the horizontal axis is the range. Comparing panel (d) to panel (e), the beam quality with fixed transmit and fixed receive focusing is significantly improved with filtering. It is also shown that the filtering technique with fixed re-

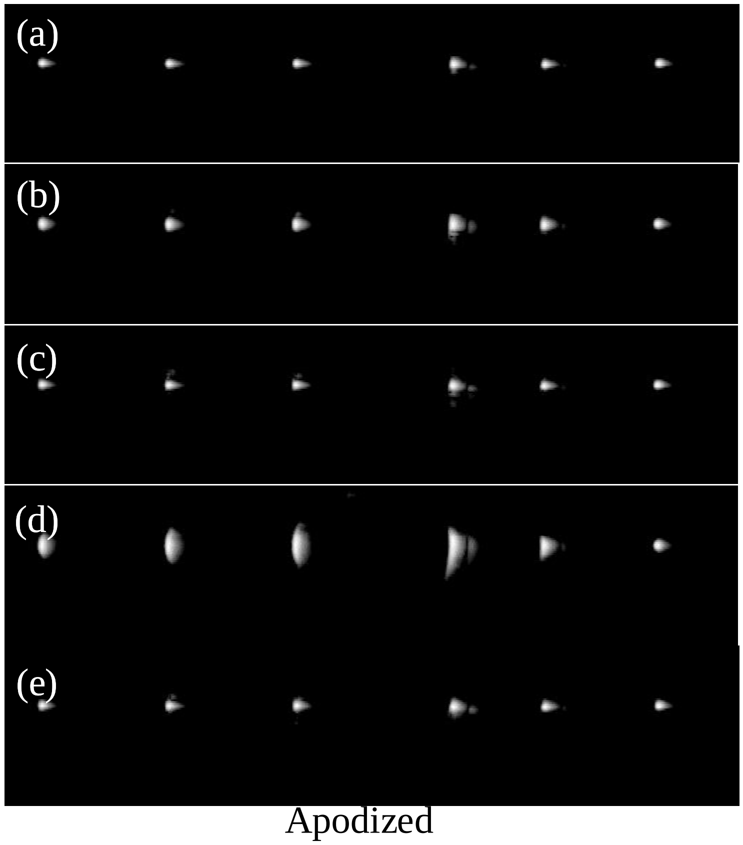

FIG. 8 Images of six wires over a 40 dB dynamic range (apodized). The vertical axis is the azimuth and the horizontal axis represents the range. (a) is dynamic transmit and dynamic receive focusing. (b) is fixed transmit focusing at 60 mm and dynamic receive focusing. (c) is (b) with the retrospective filtering technique. (d) is fixed transmit and fixed receive focusing at 60 mm. (e) is (d) with the retrospective filtering technique.

ceive focusing (panel (e)) can provide similar imaging performance to that of the image shown in panel (c) (i.e., dynamic receive focusing with filtering).

The images with apodization are shown in figure 8 with the same display format. Similar to figure 7, the beam quality with fixed transmit and fixed received focusing is still significantly improved. Moreover, the filtering technique with fixed receive focusing can still achieve imaging performance similar to that of dynamic receive focusing with filtering.

Figure 9 presents the projected beam patterns for the last wire (i.e., at 121 mm) without apodization (top) and with apodization (bottom). In both panels, dynamic transmit and dynamic receive focusing (dotted), fixed transmit and dynamic receive focusing before filtering (solid), fixed transmit and dynamic receive focusing after filtering (dot-dashed) and fixed transmit and fixed receive focusing after filtering (dashed) are demonstrated. It is shown that fixed transmit and fixed receive focusing with filtering has performance similar to that of fixed transmit and dynamic receive focusing with filtering for both the unapodized and apodized cases.

Figures 10 and 11 show results of the same wire phantom except that the fixed focus is at 120 mm. The beam patterns of the wire at 65 mm are shown in figure 12. Results are consistent with the previous results shown in figures 7, 8 and 9.

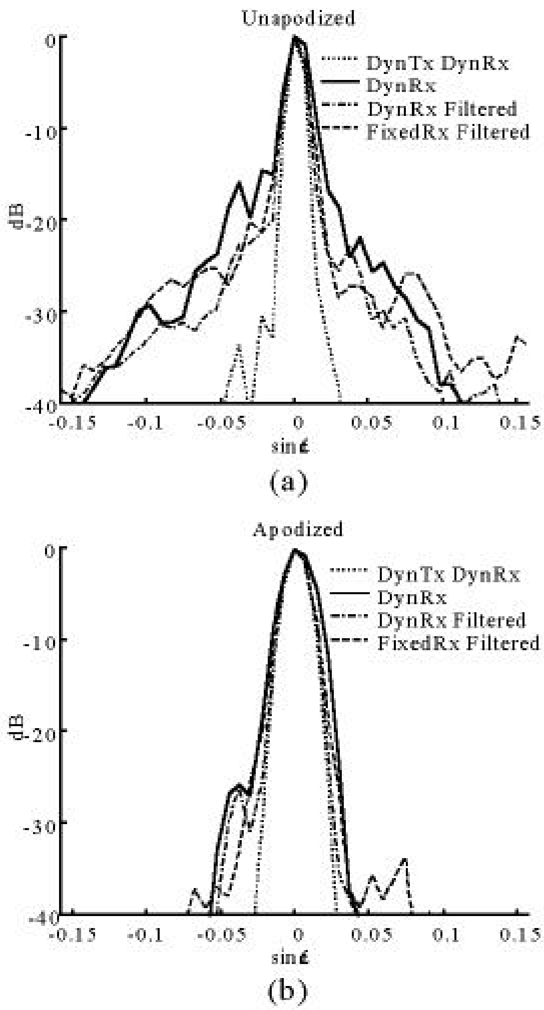

FIG. 9 Beam patterns at 121 mm. Top panel shows the unapodized cases and bottom panel corresponds to the apodized cases. Dotted line: dynamic transmit and dynamic receive focusing. Solid line: fixed transmit focusing at 60 mm and dynamic receive focusing. Dot-dashed line: fixed transmit focusing at 60 mm and dynamic receive focusing after filtering. Dashed line: fixed transmit and fixed receive focusing at 60 mm after filtering.

Data from a speckle generating phantom with anechoic cysts are also used to evaluate effectiveness of the filtering approach on contrast resolution improvement. A tissue-mimicking phantom (RMI-412R, Gammex RMI, Middleton, Wisconsin, U.S.A.) with sound velocity of 1.54 mm/ μs and an attenuation rate of 0.5 dB/cm/MHz was used. 30 dB images in the vicinity of a cyst at 65 mm are shown in figures 13 (without apodization) and 14 (with apodization). In both figures, the vertical axis is the range and the horizontal axis represents the azimuth. Panel (a) is the ideal image with dynamic transmit and dynamic receive focusing. Panels (b) and (d) are the unfiltered images corresponding to cases with fixed transmit focusing at 120 mm and dynamic receive focusing (panel (b)) and with fixed transmit and fixed receive focal depth at 120 mm (panel (d)). Panels (c) and (e) are the filtered images corresponding to panels (b) and (d), respectively. It is shown that detection of the cyst is improved for fixed receive focusing with or without apodization. The cyst detectability for fixed receive focusing with filtering is similar to that for dynamic receive focusing.

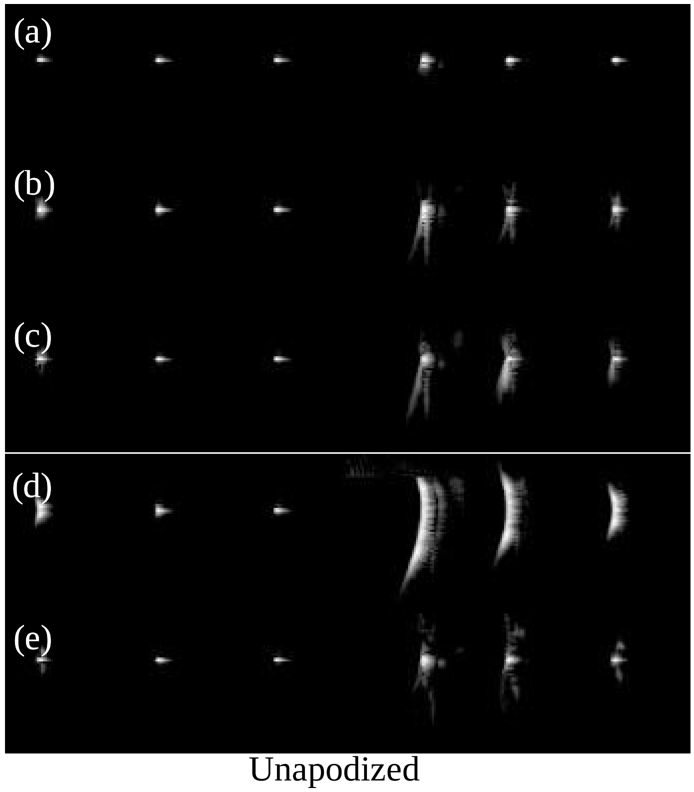

FIG. 10 Images of six wires over a 40 dB dynamic range (unapodized). The vertical axis is the azimuth and the horizontal axis represents the range. (a) is dynamic transmit and dynamic receive focusing. (b) is fixed transmit focusing at 120 mm and dynamic receive focusing. (c) is (b) with the retrospective filtering technique. (d) is fixed transmit and fixed receive focusing at 120 mm. (e) is (d) with the retrospective filtering technique.

V. CONCLUSION

In this paper, the retrospective filtering technique was extended to fixed transmit and fixed receive focusing. It was found that the technique provides image quality similar to that with dynamic receive focusing with or without apodization. The smaller amplitude variations of the apodized apertures also imply that the deconvolution process is more robust and shorter filters may be applied with similar performance. However, one disadvantage for the filtering technique with fixed receive focusing is that it needs a longer filter compared to that for dynamic receive focusing. This means that more beam lines must be acquired for fixed receive focusing to obtain the same field of view.

The other disadvantage for a long filter is the motion artifact. In particular, if the object moves by more than a quarter wavelength over the entire time needed to acquire all beams used in the retrospective processing, motion artifacts will occur.[11] As described in this paper, 21 beams are used to reconstruct one beam line for fixed receive focusing. Thus, the motion must be negligible during a period of 21 pulse repetition intervals (PRI's). For a 160 mm image depth, the object should not move by more than a quarter wavelength in a period of about 4.5 ms. This represents a velocity of about 25 mm/s. Thus, tissue motion may be significant for cardiac applications and the motion must be corrected in order to apply the filtering technique.

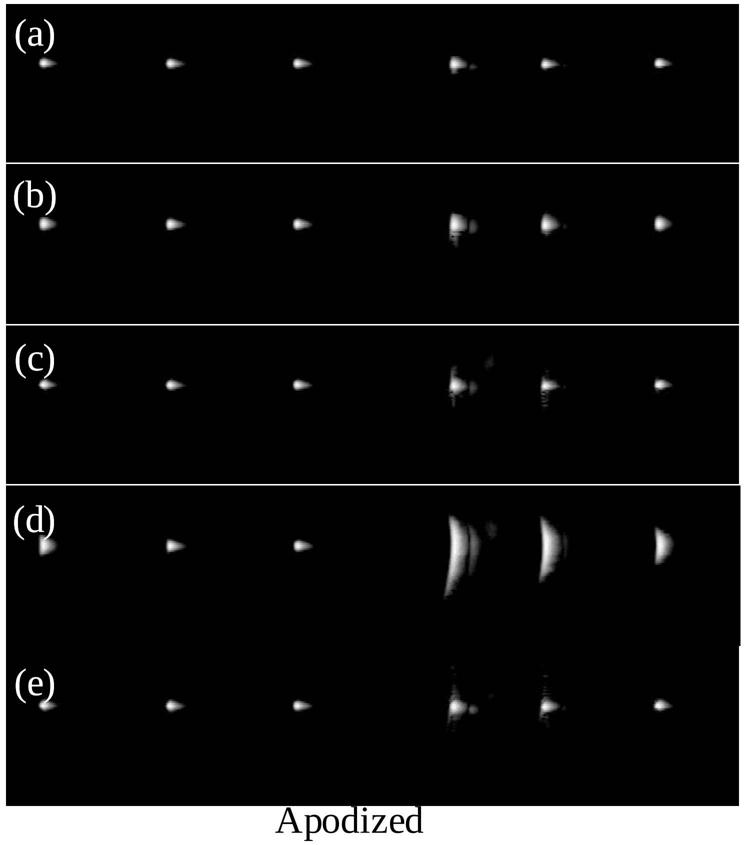

FIG. 11 Images of six wires over a 40 dB dynamic range (apodized). The vertical axis is the azimuth and the horizontal axis represents the range. (a) is dynamic transmit and dynamic receive focusing. (b) is fixed transmit focusing at 120 mm and dynamic receive focusing. (c) is (b) with the retrospective filtering technique. (d) is fixed transmit and fixed receive focusing at 120 mm. (e) is (d) with the retrospective filtering technique.

In this paper, fixed receive focusing was applied in combination with fixed receive apodization. Another possibility is to use dynamic receive apodization along with fixed receive focusing. In this case, the near field performance may be improved at the price of a slight increase in system complexity. Nonetheless, as long as the effective aperture width of a fixed focused system is larger than that of the gold standard system, the filter-based approach can achieve performance similar to that of the gold standard system. The only potential disadvantage is that a longer filter may be required for fixed apodization than that for dynamic apodization. Finally, since only fixed receive focusing is required, no real-time receive dynamic focusing circuit is needed. The complex dynamic receive focusing circuit is replaced by a simple 1-D filter bank at the beamformer output. Thus, hardware complexity is substantially reduced without sacrificing imaging performance.

ACKNOWLEDGMENTS

Data used in this paper were downloaded from the Biomedical Ultrasonics Laboratory at the University of Michigan (http://bul.eecs.umich.edu). The authors would also like to thank the reviewers for helpful comments.

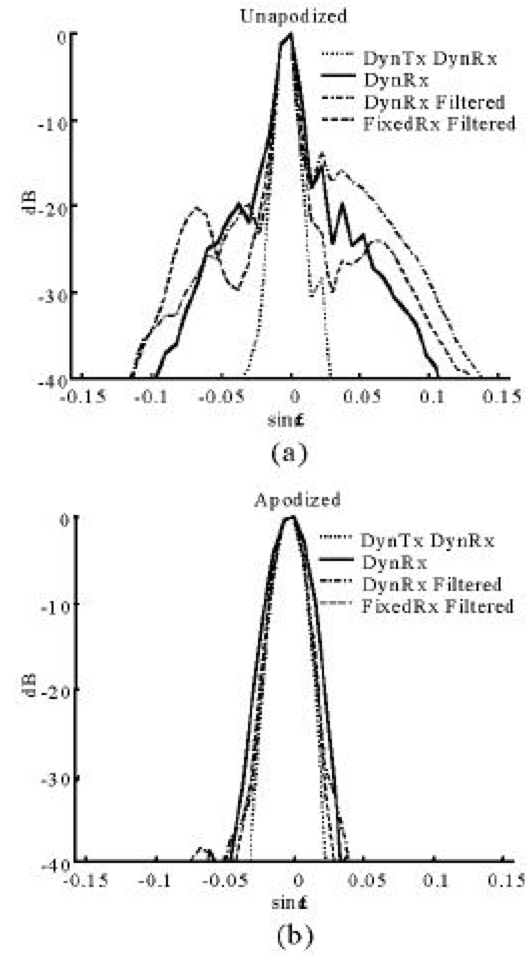

FIG. 12 Beam patterns at 65 mm. Top panel shows the unapodized cases and bottom panel corresponds to the apodized cases. Dotted line: dynamic transmit and dynamic receive focusing. Solid line: fixed transmit focusing at 120 mm and dynamic receive focusing. Dot-dashed line: fixed transmit focusing at 120 mm and dynamic receive focusing after filtering. Dashed line: fixed transmit and fixed receive focusing at 120 mm after filtering.

REFERENCES

1. Wright, J., Resolution issues in medical ultrasound, in *Proc. IEEE Ultrasonics Symp.* , pp. 793-799 (1985).

2. Lu, J.Y. and Greenleaf, J., Ultrasonic nondiffracting transducer for medical imaging, *IEEE Trans. Ultrason. Ferroelect. Freq. Contr. 37*, 438-447 (1990).

3. Lu, J.Y. and Greenleaf, J., Sidelobe reduction for limited diffraction pulse –echo systems, *IEEE Trans. Ultrason. Ferroelect. Freq. Contr. 40*, 735-746 (1993).

4. Lu, J.Y., Designing limited diffraction beams, *IEEE Trans. Ultrason. Ferroelect. Freq. Contr. 44*, 181-193 (1997).

5. Shen, J. and Ebbini, E.S., A new coded-excitation ultrasound imaging system – part I: basic principles, *IEEE Trans. Ultrason. Ferroelect. Freq. Contr. 43*, 131-140 (1996).

6. Shen, J. and Ebbini, E.S., A new coded-excitation ultrasound imaging system – part II: operator design, *IEEE Trans. Ultrason. Ferroelect. Freq. Contr. 43*, 141-148 (1996).

7. Haider, B., Synthetic transmit focusing for ultrasonic imaging, in *Proc. IEEE Ultrasonics Symp.*, pp. 1215-1218 (2000).

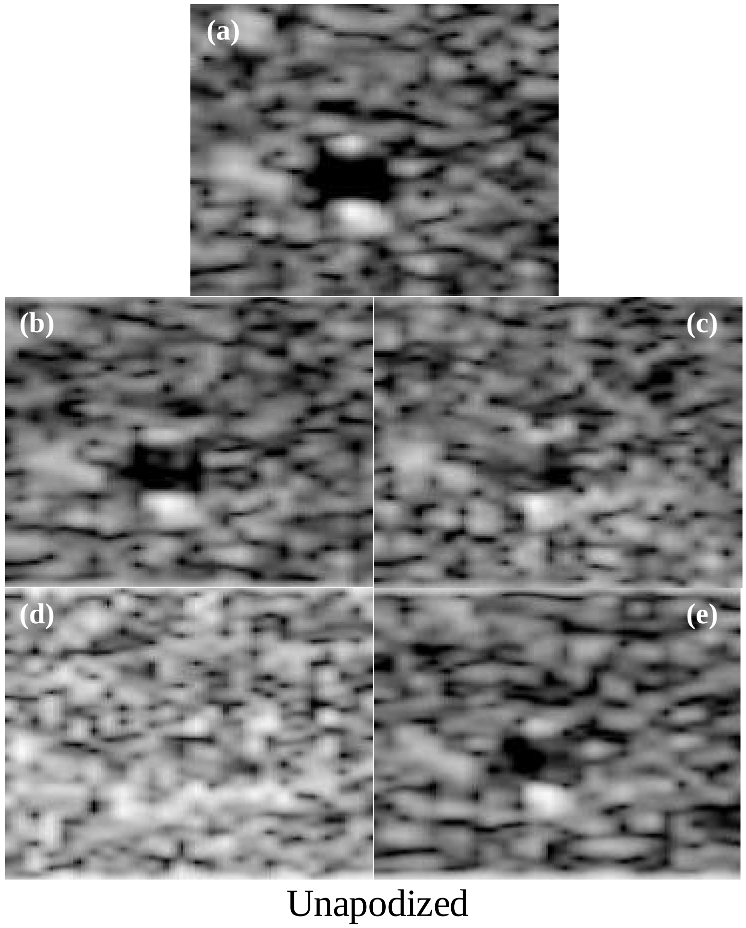

FIG. 13 30 dB images of the anechoic cyst in a tissue-mimicking phantom (unapodized). The vertical axis is the range and the horizontal axis is the azimuth. (a) is dynamic transmit and dynamic receive focusing. (b) is fixed transmit focusing at 120 mm and dynamic receive focusing. (c) is (b) with the retrospective filtering technique. (d) is fixed transmit and fixed receive focusing at 120 mm. (e) is (d) with the retrospective filtering technique.

8. Robinson, B. and Cooley, C., Synthetic dynamic transmit focus, in *Proc. IEEE Ultrasonics Symp.*, pp. 1209-1214 (2000).

9. Bae, M.H. and Jeong, M.K., A study of synthetic-aperture imaging with virtual source elements in B-mode ultrasound imaging systems, *IEEE Trans. Ultrason. Ferroelect. Freq. Contr. 47*, 1510-1518 (2000).

10. Freeman, S., Li, P.C. and O'Donnell, M., Retrospective dynamic transmit focusing, *Ultrasonic Imaging 17*, 173-196 (1995).

11. O'Donnell, M. and Thomas, L.J., Efficient synthetic aperture imaging from a circular aperture with possible application to catheter-based imaging, *IEEE Trans. Ultrason. Ferroelect. Freq. Contr. 39*, 366-380 (1992).

12. Li, P.C. and O'Donnell, M., Synthetic aperture imaging using a Lagrange based filtering technique, *Ultrasonic Imaging 14*, 354-366 (1992).

13. Li, P.C., Pulse compression for finite amplitude distortion based harmonic imaging using coded waveforms, *Ultrasonic Imaging 21*, 1-16 (1999).

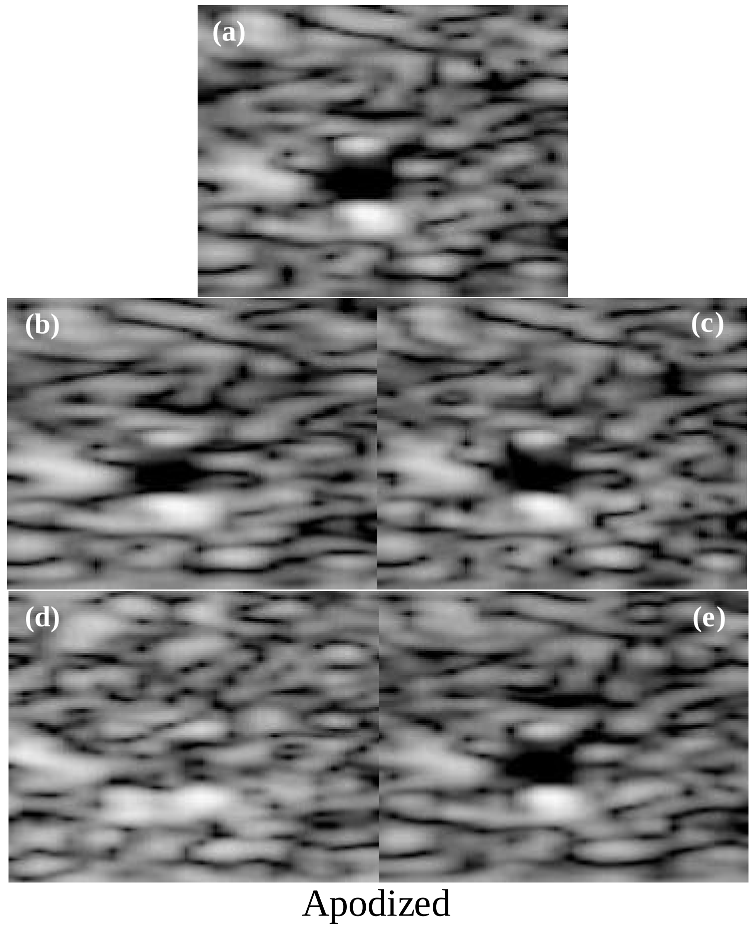

FIG. 14 30 dB images of the anechoic cyst in a tissue-mimicking phantom (apodized). The vertical axis is the range and the horizontal axis is the azimuth. (a) is dynamic transmit and dynamic receive focusing. (b) is fixed transmit focusing at 120 mm and dynamic receive focusing. (c) is (b) with the retrospective filtering technique. (d) is fixed transmit and fixed receive focusing at 120 mm. (e) is (d) with the retrospective filtering technique.